NRC·CNRC

NRC Publications Archive
Archives des publications du CNRC

Tomographic measurement of buried interface roughness

Hayashida, Misa; Ogawa, Shinichi; Malac, Marek

This publication could be one of several versions: author's original, accepted manuscript or the publisher's version. / La version de cette publication peut être l'une des suivantes : la version prépublication de l'auteur, la version acceptée du manuscrit ou la version de l'éditeur.
For the publisher's version, please access the DOI link below./ Pour consulter la version de l'éditeur, utilisez le lien DOI ci-dessous.

Publisher's version / Version de l'éditeur:
https://doi.org/10.1116/1.4926975
Journal of Vacuum Science and Technology B, Nanotechnology and Microelectronics: Materials, Processing, Measurement, and Phenomena, 33, 4, pp. 1-6, 2015-07-22

NRC Publications Archive Record / Notice des Archives des publications du CNRC :
https://nrc-publications.canada.ca/eng/view/object/?id=e36f6c00-b551-437e-a752-9b64a57b527a
https://publications-cnrc.canada.ca/fra/voir/objet/?id=e36f6c00-b551-437e-a752-9b64a57b527a

Access and use of this website and the material on it are subject to the Terms and Conditions set forth at
https://nrc-publications.canada.ca/eng/copyright
READ THESE TERMS AND CONDITIONS CAREFULLY BEFORE USING THIS WEBSITE.

L'accès à ce site Web et l'utilisation de son contenu sont assujettis aux conditions présentées dans le site
https://publications-cnrc.canada.ca/fra/droits
LISEZ CES CONDITIONS ATTENTIVEMENT AVANT D'UTILISER CE SITE WEB.

Questions? Contact the NRC Publications Archive team at PublicationsArchive-ArchivesPublications@nrc-cnrc.gc.ca. If you wish to email the authors directly, please see the first page of the publication for their contact information.

Vous avez des questions? Nous pouvons vous aider. Pour communiquer directement avec un auteur, consultez la première page de la revue dans laquelle son article a été publié afin de trouver ses coordonnées. Si vous n'arrivez pas à les repérer, communiquez avec nous à PublicationsArchive-ArchivesPublications@nrc-cnrc.gc.ca.

National Research Council Canada | Conseil national de recherches Canada

Canada

Tomographic measurement of buried interface roughness

Misa Hayashida[a)]
National Metrology Institute of Japan, National Institute of Advanced Industrial Science and Technology (AIST), 1-1-1, Higashi, Tsukuba, Ibaraki 305-8565, Japan and National Institute of Nanotechnology (NINT), 11421 Saskatchewan Drive, Edmonton, Alberta T6G 2M9, Canada

Shinichi Ogawa
Nanoelectronics Research Institute, AIST, 16-1 Onogawa, Tsukuba, Ibaraki 305-8569, Japan

Marek Malac
NINT, 11421 Saskatchewan Drive, Edmonton, Alberta T6G 2M9, Canada and Department of Physics, University of Alberta, Edmonton, Alberta T6G 2E1, Canada

(Received 23 March 2015; accepted 7 July 2015; published 22 July 2015)

The authors demonstrate that electron tomography allows accurate measurement of roughness of buried interfaces in multilayer samples. The method does not require the interface to be exposed at the surface of the sample, or does it require a laterally extended sample. Therefore, it enables quantitative site specific analysis of individual elements within semiconductor devices. The standard deviation of the interface distance from a plane fitted to an interface is used as a measure of the interface roughness. The roughness is evaluated in three dimensions, eliminating the uncertainties inherent to roughness measurements on cross-sectional images from a single projection. The apparent interface roughness depends on the signal-to-noise ratio (S/N) arising from electron counting statistics in the data. To eliminate the effect of the S/N, multiple images were collected at each tilt. The roughness was extrapolated to an asymptotic value with a high S/N. This value was taken as the true interface roughness. The method was validated on computer generated data by demonstrating a good agreement between known roughness values and asymptotic values obtained using the above method. [http://dx.doi.org/10.1116/1.4926975]

I. INTRODUCTION

Interface roughness of buried layers in nanometer size devices often degrades performance of the devices because the roughness of the interfaces might affect expected growth of consequent layers during the device fabrication. To characterize the roughness of an exposed surface, atomic force microscope (AFM)[1] has been widely used. Small angle x-ray scattering can be used to measure average roughness of either laterally extended interfaces or interfaces within periodic structures.[2] In practice, it is desirable to quantitatively evaluate roughness of buried interfaces on a sample containing multiple layers within a localized area of devices with small, frequently sub-100 nm, lateral dimensions. Often a single defective structure within a device needs to be analyzed with as little distortions as possible.

A transmission electron microscope (TEM) or a scanning TEM (STEM) can be used to observe the roughness of a cross section of a sample directly. To allow for high resolution image acquisition, the sample must be made very thin in a focused ion beam instrument (FIB). A very thin sample may bend or the device features may be damaged during the FIB fabrication. When a single cross section is used, the information about the sample is integrated along the electron beam path in the (S)TEM giving only beam path-averaged roughness. A true roughness of the buried interface in three dimensions (3D), comparable to an AFM roughness measurement of exposed surfaces, is needed to provide insights into device fabrication and defect issues.

Electron tomography in a (S)TEM[3,4] can retrieve a 3D volume reconstruction from a series of two-dimensional projection images acquired at suitable tilt increments. Zhong *et al.*[5] reported a protocol to quantitatively measure the roughness of ZrO_2/In_2O_3 multilayer films from a 3D volume obtained from energy-filtering TEM tomography. It is difficult to estimate reliability and accuracy of a roughness measurement method when working with experimental data only. To obtain an estimate of the reliability and accuracy, it is desirable to benchmark the method on computer-generated data with known interface roughness values. Similarly, the computer generated data can be used to gain insights into the effect of shot noise in the images and, as reported here, the error arising from the process of roughness extrapolation to a high dose.

Here, we present an electron tomography method for the evaluation of buried interface roughness of SiO_2/W multilayer films using annular dark field (ADF) STEM mode. We detected the location of the interface using median filter, low pass filter, Sobel filter, and binary filter. To verify the performance of the image processing procedure, we also evaluated roughness of computer generated test data and obtained a good agreement between the known input roughness and the roughness obtained using our data processing procedure. We also investigated the effect of the S/N in the images on the calculated roughness value accuracy.

[a)]Electronic mail: Misa.Hayashida@nrc-cnrc.gc.ca

II. SAMPLE PREPARATION AND DATA ACQUISITION

Figure 1(a) shows a rod-shaped specimen[6] fabricated from a multilayer test sample used to demonstrate the roughness evaluation. The sample was grown as a sequence of SiO_2–W–SiO_2 on a Si wafer. The SiO_2-on-W interface [upper part of Fig. 1(a)] exhibits higher roughness than the deeper W-on-SiO_2 [lower part of Fig. 1(a)]. The rod-shaped sample was fabricated using a Hitachi NB 5000 dual beam (FIB/SEM) instrument. Nanodot fiducial markers[7] for alignment of the tilt series were fabricated by SEM with gas injection system in the same instrument. The tilt series was acquired using ADF STEM mode of a Hitachi HF-3300 TEM/STEM with cold field emission source and the MAESTRO computer control system.[8] We used free lens control mode to adjust collection angle of the ADF detector. To do that, the projector lens excitation was adjusted to maximize the intensity of the collected ADF signal while excluding diffraction contrast. The tilt step was 3° over the entire 180° tilt range eliminating the missing wedge problem. At every tilt, ten images were collected with 5 μs/pix dwell time to reduce the effect of sample drift and to evaluate the effect of the S/N. Beam current was between about 5 and 10 pA. The images were summed after compensating for drift using standard cross correlation alignment. To evaluate the effect of the S/N, a subset of 3, 5, 7, and 10 projected images were summed at each tilt resulting in four tilt series with increasing incident electron dose. The images were 512×1024 pixels with $(0.47\,\text{nm})^2$ pixel size. To align the images within the tilt series for the four dose series, the nanodot fiducial marker method was used.[7] The RMS difference[7] between the expected and measured marker position in the projected images over the entire tilt series was 1.84 pixels that is 0.86 nm.

All four tilt series at various doses were reconstructed using filtered back projection.[9] Figure 1(b) shows the 3D volume rendering of the sample. The damage by the electron beam during the acquisition is negligible as judged by absence of observable changes between the first (0°) and last (180°) images in the tilt series.

III. IMAGE PROCESSING

To detect the location of the interface, median filter, low pass filter, Sobel filter, and binary filter were subsequently applied to the slice images as shown in Figs. 1(c) and 1(d). The same filters with the same parameters (except for the threshold of the binary filter) were applied to both experimental images and computer generated images. In this way, the computer generated data were used to validate the data processing step of the roughness measurement.

Median filter (window size 7 pixels) was used to decrease the effect of shot noise in the images. The low pass filter (window size 10 pixels) and Sobel filter were used to enhance the interface visibility after contrast adjustment of

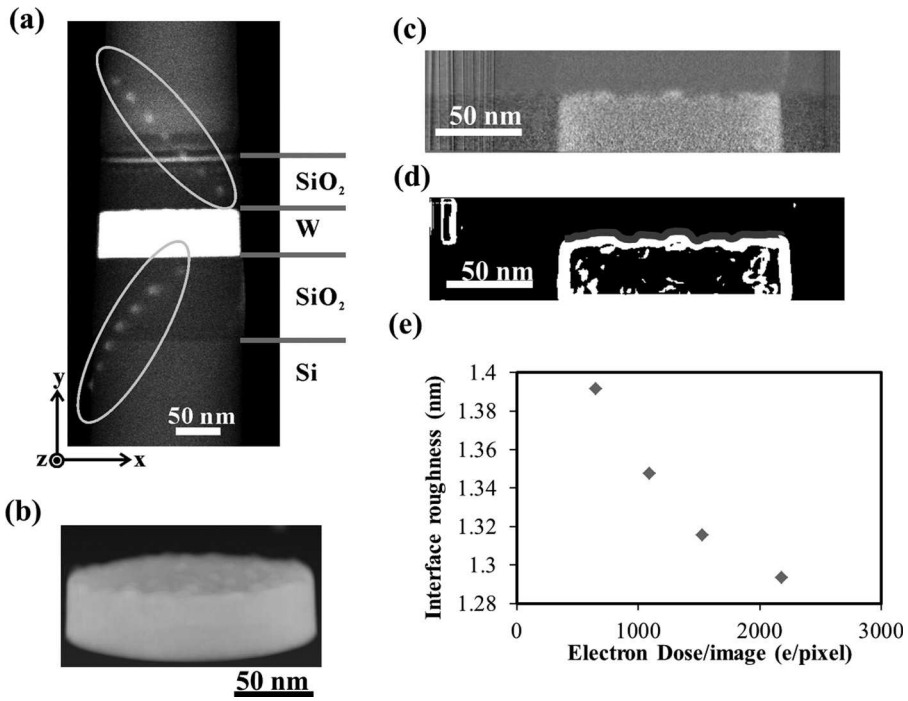

FIG. 1. (a) Experimental ADF STEM image of the (from top) SiO_2–W–SiO_2 on silicon wafer test sample used for evaluation of interface roughness. The fabricated nanodot fiducial markers are indicated by the two ellipses. The upper SiO_2-on-W interface was used for this work. To enhance the markers' contrast, the brightness of W part is saturated. (b) The 3D volume rendering of the sample. (c) Z slice section of the reconstructed volume. (d) A processed image allowing the detection of the SiO_2-on-W–SiO_2 interface. The gray line indicates the interface between SiO_2 and W layer. (e) The experimental relationship between measured roughness and electron dose. The horizontal axis is the incident number electrons per pixel for each image of a tilt series. Ten images were collected at each tilt allowing us to generate tilt series with 3, 5, 7, and 10 images summed at each tilt. The apparent interface roughness decreases with increasing S/N and tends to an asymptotic value of 1.1 nm at a high irradiation dose.

each image. The binary filter was used to convert the reconstructed data volume into binary images. Then, the position of the boundary (interface) between black (digital 0) and white (digital 1) were detected in each slice parallel to the sample's long axis (Z slice). The window sizes of the median filter and the low pass filter were adjusted to the smallest value that keeps the interface continuous, as shown in Fig. 1(d). Decreasing the window size further leads to the presence of discontinuities at the interface. Increasing the window size leads to excessive smoothing and the measured interface roughness becomes lower than the known interface roughness in the computer-generated data. In this way, we estimated the appropriate window size by utilizing computer generated tilt series data with varying electron dose.

Approximately 7×10^4 points were detected in every tilt series. A plane that minimizes the RMS distance from the interface was fitted to the interface in the 3D reconstructed volume. The plane corresponds to the mean position of the buried interface as estimated by minimizing the RMS deviations. The standard deviation of distances from this fitted plane was taken as the interface roughness. The same processing was applied to all four experimental tilt series and to the computer generated test data.

IV. RESULT

Figure 1(e) shows that the apparent value of the interface roughness decreases with increasing electron dose in the experimental data. This is because the S/N increases with increasing electron dose which in turn improves the image processing accuracy. Furthermore, Fig. 1(d) shows that the apparent interface roughness tends to an asymptotic value with increasing electron dose. Since we have generated four experimental tilt series, we can extrapolate the measured data and estimate the asymptotic interface roughness at a high S/N. To do that, the experimental dose dependence of roughness in Fig. 1(e) is fitted to a power law as follows:

$$IR(q) = \boldsymbol{a}q^{-\boldsymbol{b}} + \boldsymbol{d}, \tag{1}$$

where $IR(q)$ is the interface roughness as a function of dose q in counts and $\boldsymbol{a}$, $\boldsymbol{b}$, and $\boldsymbol{d}$ are constants. At high dose, $q \to \infty$, the interface roughness tends toward the constant $\boldsymbol{d}$, which represents the interface roughness at high dose. While the true value of the interface roughness in an experimental sample is not known, it appears to be reasonable to take the asymptotic value ($\boldsymbol{d}$) as the true representation of the interface roughness, about 1.1 nm in the example shown in Fig. 2.

V. SIMULATION

To verify the image processing step, we evaluated the roughness of computer generated test data. Many virtual tilt series with varying S/N and contrast levels were generated. In an experiment, these parameters would correspond to variation in incident electron dose (S/N) and the collection angle in STEM mode or the objective aperture in TEM mode (both affecting the contrast). Varying levels of roughness were simulated as well. Each data set was 512×256 pixels, and angular step in the computer generated tilt series was 3° over ±90° tilt range to match our experimental data. The data were intended to simulate the STEM annular dark field mode used in the experiments above.

The images consist of a bright region (tungsten), a dark region (SiO_2), and zero region (vacuum outside sample), as shown in Fig. 2(a) with the evaluated interface between the W and SiO_2 region, marked by a dashed line. The S/N was evaluated in the SiO_2 region of the sample as the standard deviation divided by mean brightness in the SiO_2 region. The equivalent dose for simulated images was estimated by adjusting the S/N in the SiO_2 region to match the experimental data. The effect of contrast (C) difference between the reference region SiO_2 and the tungsten region in a projection image was investigated by generating images with W region contrast that is 2, 5, 10, and 20 times higher than the contrast in the reference SiO_2 region. The shot noise in the computer generated projection images was implemented by a randomly generated number of incident electrons at each pixel multiplied by the projected sample thickness and contrast at each pixel. The number of incident electrons N per pixel at each image was taken 30, 50, 100, 200, 500, 1000, 3000, and 5000. For example, when an electron was incident on tungsten region with thickness t and contrast $C = 2$, we assumed that $t*C$ counts were detected at that pixel.

In STEM mode, the measured intensity per pixel is related to the incident electron dose in a complicated way.[10] Therefore, we calibrate the incident electron dose of simulation data empirically using the known collection parameters of the experimental data. As shown in Figs. 3(a) and 3(b), we evaluated the statistical mean and standard deviation in both experimental images and computer generated images. Then, we calculated the S/N as standard deviation divided by the statistical mean in the SiO_2 region. In the experimental data, when the collected electron dose estimated from the known beam current and pixel dwell time was 2180 electrons/pixel, the S/N ratio was 0.056. We converted the S/N of simulation tilt series to electron dose using 2180/0.056 * SNC, here SNC is the calculated S/N of the computer generated image.

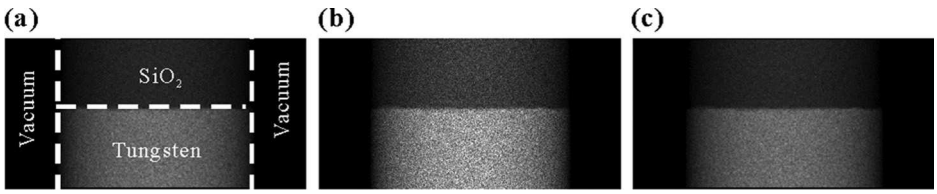

FIG. 2. (a) Example projection image from a computer generated virtual tilt series. (b) and (c) Computer generated images before and after Gaussian filter. The application of a Gaussian filter as shown in (c) more closely resembles the experimental images as shown in Fig. 3(b). Each data set is 512×256 pixels.

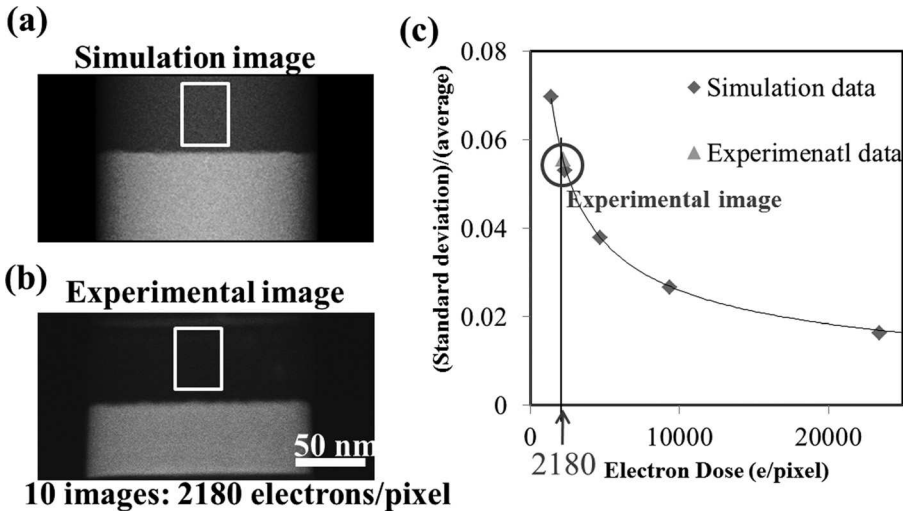

FIG. 3. (a) and (b) Areas of SiO_2 used for calibration from counts to electron dose in an image. The image size of the simulation image is 512 × 256 pixels. (c) The relationship between S/N ratio and electron dose at each image.

The results are shown in Fig. 3(c). For example, for $N = 100$, the S/N is 0.038 and the incident electron dose is 4687 electrons/pixel. The computer-generated tilt series was reconstructed in exactly the same manner as the experimental data.

Figure 2(b) is an example of a computer generated projected image. The image has higher spatial frequency component compared with an experimental image in Fig. 3(b). To provide insight in the experiment, the simulations need to closely reflect the parameters used in the experiments. The critical parameters in the experiment are the probe size and probe broadening, and the S/N in the data. The probe size and probe broadening derive both from probe geometry and from interactions of the electron beam with the sample.[11] To account for the probe broadening, we applied a Gaussian filter to the computer generated projection images. The filter with a window size of 3 pixels was as follows:

$$\begin{bmatrix} 1/16 & 2/16 & 1/16 \\ 2/16 & 4/16 & 2/16 \\ 1/16 & 2/16 & 1/16 \end{bmatrix}. \quad (2)$$

The pixel size of experimental tilt series was 0.47 nm. Therefore, the broadening as described by Eq. (2) is about 1.4 nm. After the filter was applied to the computer-generated projected images, the images, as shown in Fig. 2(c), resembled the experimental tilt series more closely.

The generated tilt series were then reconstructed and the interface between SiO_2 and W parts of Z-slice images was detected using the same method as the experimental data. Figure 4(a) shows the relation between incident electron dose and roughness measured from four computer generated tilt series with different input roughness. A contrast level of $C = 20$, which is close to the contrast in the experimental data, was used. The input roughness is indicated by the solid horizontal line for each input value. In agreement with the experiment, the roughness estimated from the series is getting closer to known input roughness with increasing electron dose. Figure 4(b) shows the relation between S/N and roughness for various contrast levels. The black line indicates the known input interface roughness, 2.7 pixels. Not surprisingly, the agreement between the known input roughness and the estimated one improves as the S/N and contrast increase.

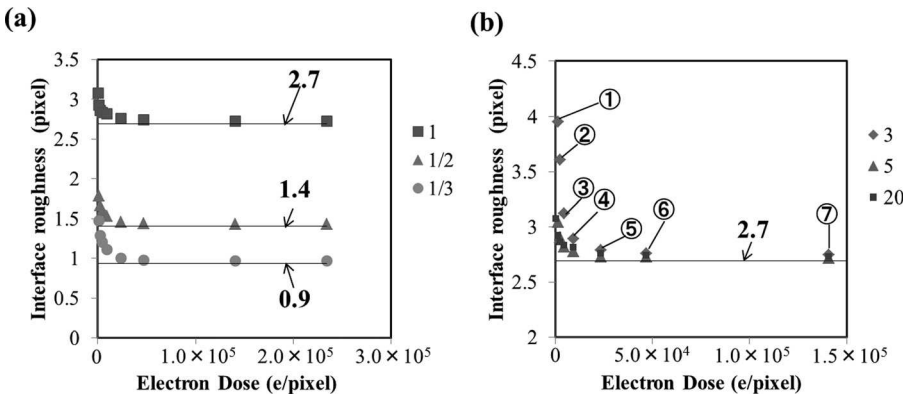

FIG. 4. Relation between measured roughness from computer-generated tilt series and electron dose with different roughness (a) and with different contrast (b). In (a), the known input roughness was 2.7 pixels, 1.4 pixel and 0.9 pixels. The contrast used for the simulation was $C = 20$ that is close to the experimental data. The dose dependence of the apparent roughness for known input roughness taken as 2.7 pixels.

VI. DISCUSSION

The measurement of a buried interface's roughness on device sections with small lateral dimensions is important for device failure characterization and for development of new devices. Electron tomography, as presented here, provides a means to measure approximate interface roughness within about 1 nm on ~100–200 nm diameter rod shaped sections. If a tilt series of the sample with $^1/_2$ the pixel size as compared to here $(0.47\,\text{nm})^2$ was collected, the resolution in the reconstructed volume would improve correspondingly assuming that the alignment, probe size, broadening, and sample drift do not limit the resolution. Since the probe size (less than 0.3 nm) is smaller than the pixel size (~0.5 nm), it is expected that the lower interface roughness, below 1 nm, can be measured. However, the broadening of the electron beam within the sample could exceed the pixel size if the sample rod diameter is large. The beam broadening arises both from probe geometry and from broadening due to electron scattering in the sample. A rough estimate indicates that geometrical broadening δd of the probe propagating through the 100 nm diameter rod with 10 mrad incidence angle is about $\delta d = (10\ \text{mrad})*(100\,\text{nm}/2) = 0.5\,\text{nm}$, assuming that the probe is focused at the midplane of the sample (at $^1/_2$ diameter: d). This provides a lower estimate for broadening of the experimental data. In practice, it is difficult to focus the probe exactly at the midplane, and the broadening due to both elastic and inelastic scattering must be also included.[11] This leads to a 3 pixel (1.4 nm) Gaussian being used to smear out the detail in the computer generated data.

The amount of geometrical broadening depends only on the probe geometry. It is well known that decreasing the probe diameter requires increasing the convergence angle,[10,12] which in turn leads to increased geometrical broadening. To limit the geometrical broadening to a value δd, the rod diameter D and the probe convergence angle α should satisfy the relation $2\alpha/D < \delta d$. The estimate of broadening due to both elastic and inelastic scattering depends on collection parameters in a rather complicated way. As rule of thumb, the broadening due to scattering increases with increasing projected mass thickness of the examined rod. The 150 nm diameter rod used here has a mass thickness of about $300\,\text{mg/cm}^2$ in the tungsten part and about $40\,\text{mg/cm}^2$ in the SiO_2 region. This indicates that for most samples of practical interest examined at ~1 nm resolution, the broadening due to electron scattering is not a limiting factor.

Therefore, a small diameter rod should be fabricated in FIB to decrease the effect of probe broadening. The decrease in pixel size however corresponds to increase in electron dose. For example, if the S/N is to be kept the same in the experimental images, the decrease of pixel size by a factor $^1/_2$ corresponds to an increase in irradiation dose by a factor of four. The resulting electron beam irradiation damage can then become the main factor limiting the achievable resolution for many materials. The ultimate resolution of the method is therefore difficult to estimate. Assuming that technical limitations, such as fabrication of small diameter, sample drift, and alignment accuracy, can be circumvented, the electron irradiation damage and perhaps the large convergence angle of instruments forming small STEM probe (and associated geometrical broadening in practical samples) determine the achievable resolution.

The extrapolation of the roughness to an asymptotic value at a high dose eliminates the dependence of the measured roughness on the incident dose. However, the irradiation damage increases with increasing electron dose. If the interface is modified by the damage, it could be expected that the interface roughness should be decreasing (becoming more smooth) with increasing dose. Therefore, the question remains on what is the most suitable approach to execute the extrapolation and what is the minimum suitable data set needed (that is, electron dose and number of dose series).

The extrapolation of roughness to a high dose needs to be treated cautiously. As any extrapolation, the process is prone to amplifying the effect of any inaccuracies and small number of fitting points. Testing the process on computer generated data with known value of roughness can help to determine the conditions under which the extrapolation may be possible. Table I shows example fit parameters a, b, and d in Eq. (1) for the simulated tilt series with contrast $C = 3$ in Fig. 4(b). The known input roughness in the data set was 2.7 pixels. For practical purposes, it is the number of points in the dose dependence, i.e., the number of tilt series that need to be evaluated, that is the most time consuming step. It appears that the estimate of asymptotic roughness from seven points yields asymptotic roughness ($\boldsymbol{d}$) ~2.7 pixels, in good agreement with the known input value. The asymptotic roughness from four points was 2.2 pixels. The difference from the known value of the interface roughness in the computer-generated data is 0.5 pixels. If the pixel size is same as our experimental data (0.47 nm/pixel), the interface roughness in the experimental data (2.7 pixels) and the difference from the true value should be no more than 0.5 pixels, corresponding to 1.30 and 0.24 nm, respectively. It would therefore appear that at least four tilt series (i.e., four different doses per tilt) should be collected to obtain an acceptable estimate of the asymptotic roughness. While it may appear advantageous to collect many images at every tilt, the advantage in improving the fit of the asymptotic value may be reduced by the need increase the irradiation damage of the sample. If the dose per image is too low, the S/N can become too low for accurate alignment of both individual images at each tilt as well as for accurate alignment of the images within tilt series.

TABLE I. Example fit parameters a, b, and d in Eq. (1) for the simulated tilt series with contrast $C = 3$ in Fig. 4(b).

Number of used tilt series for fitting	$\boldsymbol{a}$	$\boldsymbol{b}$	$\boldsymbol{d}$ (pixels)
4(①–④)	68.1	0.5	2.2
5(①–⑤)	497.8	0.8	2.7
7(①–⑦)	779.4	0.9	2.7

VII. CONCLUSIONS

We have demonstrated an electron tomography method for quantitative measurement of buried interface roughness. The method allows us to measure a SiO_2-on-W interface with approximately 1 nm interface roughness. The method requires acquisition of multiple images at every tilt step during the tilt series acquisition. Several tilt series with increasing S/N are then generated by aligning and summing a subset of the images at each tilt. Reconstructing such series with increasing S/N allows us to extrapolate the roughness to an asymptotic value at high S/N. The asymptotic value is taken as the true value of the buried interface roughness, eliminating the apparent dependence of the measured interface roughness on incident dose. The method was validated on computer generated data, achieving a good agreement between the known input value of roughness and the asymptotic value obtained using the above method.

ACKNOWLEDGMENTS

The authors would like to thank Michael Bergen of NINT for useful discussion. Financial support of Visiting Researcher grant from Alberta Innovates Technology Futures is gratefully acknowledged. This work was done while the first author worked at AIST and before she moved to NINT.

[1]Y. Chen and W. Huang, Meas. Sci. Technol. **15**, 2005 (2004).
[2]T. Hofmann, E. Dobisz, and B. M. Ocko, J. Vac. Sci. Technol. B **27**, 3238 (2009).
[3]P. A. Midgley and M. Weyland, Ultramicroscopy **96**, 413 (2003).
[4]J. Fernandez, Curr. Opin. Solid Mater. Sci. **17**, 93 (2013).
[5]X. Y. Zhong, B. Kabius, D. K. Schreiber, J. A. Eastman, D. D. Fong, and A. K. Petford-Long, Appl. Phys. Lett. **100**, 101604 (2012).
[6]N. Kawase, M. Kato, H. Nishioka, and H. Jinnai, Ultramicroscopy **107**, 8 (2007).
[7]M. Hayashida, M. Malac, M. Bergen, and P. Li, Ultramicroscopy **144**, 50 (2014).
[8]M. Bergen, R. A. McLeod, M. Malac, D. Hoyle, Y. Taniguchi, T. Yaguchi, J. Chen, and T. Yotsuji, Microsc. Microanal. **19**, S1394 (2013).
[9]J. Frank, *Three-Dimensional Electron Microscopy of Macromolecular Assemblies* (Academic, San Diego, CA, 1996).
[10]L. Reimer and H. Kohl, *Transmission Electron Microscopy*, 5th ed. (Springer, Berlin, 2008).
[11]R. Egerton, Ultramicroscopy **107**, 575 (2007).
[12]O. L. Krivanek, G. J. Corbin, N. Dellby, B. F. Elston, R. J. Keyse, M. F. Murfitt, C. S. Own, Z. S. Szilagyi, and J. W. Woodruff, Ultramicroscopy **108**, 179 (2008).